AIAA JOURNAL
Vol. 49, No. 8, August 2011

Analysis of Conformable Pressure Vessels: Introducing the Multibubble

F. J. J. M. M. Geuskens,* O. K. Bergsma,† S. Koussios,† and A. Beukers‡
Delft University of Technology, 2629 HS Delft, The Netherlands

DOI: 10.2514/1.J050822

This paper outlines the structural analysis of an articulated pressurizable structure termed the *multibubble*. The multibubble is a structurally efficient pressure vessel that pressurizes a volume with substantial spatial freedom. Applications are found in pressure cabins for blended-wing–body aircraft and conformable pressure vessels for liquid gases (e.g., propane) or cryogenic applications. The multibubble in this paper can be configured in an open- or closed-cell configuration and consists of cylindrical and spherical membrane elements equipped with walls and/or reinforcements at the intersections in order to ensure structural integrity. The multibubble allows pressurization loads to be carried through in-plane stresses. To solve for loads and forces in the multibubble, it is shown that the solution simply depends on pressure and geometric variables.

Nomenclature

A	=	cross-sectional area
F_R	=	resultant membrane force
F_x	=	X component of the resultant membrane force F_R
F_y	=	Y component of the resultant membrane force F_R
$F_{\phi,c}$	=	resultant membrane force at the intersection of the multicylinder (membrane force in the wall)
$F_{\phi,s}$	=	resultant membrane force at the intersection of the multisphere
m	=	mass empty pressure vessel
N_x	=	axial membrane force
N_θ	=	hoop membrane force
N_ϕ	=	circumferential membrane force
p	=	pressure
R	=	radius
T	=	tensile load in reinforcement or reinforcement ring
U	=	transversal component of load T
V	=	axial component of load T, volume pressure vessel
$\|xx\|$	=	distance between two points
$[xxx]$	=	area of the triangle governed by three points
$[xxxx]$	=	area of the rectangle/trapezium governed by four points
ρ	=	density material pressure vessel
$\sigma_{1,2}$	=	allowable (plane) stress in the $1/2$ direction
ϕ	=	angle

I. Introduction

THERE are many applications where volume needs to be pressurized within a geometrical space for which a cylindrical or spherical vessel does not always provide suitable solutions. The main applications of interest are applications in which the pressure vessel needs to provide usable space [e.g., a structurally efficient pressure cabin for blended wing–bodies [1–3] (Fig. 1)] and applications for which the medium inside the pressure vessel cannot be compressed, because it is in a liquid state [e.g., cryogenic pressure tanks [4] (Fig. 2) or propane tanks].

Multibubbles are particularly interesting for aerospace applications, because there are strong restrictions (mainly aerodynamic related) on the geometrical space where these pressure vessels will be used.

In 1944, Jackson and Stone [5] patented a design termed *intersecting spherical pressure tanks*, in 1962 Bert [6] investigated the intersecting spherical pressure tank for aerospace applications, and in 1970 Komarov [7] published the analysis for the intersecting spherical pressure tank or the multicell reservoir [8] (Fig. 3). The reason that spherical membrane elements were chosen is because the complete structure was in uniform equal biaxial tension. Equal biaxial loading is the most efficient way of loading isotropic materials, which were the main materials for highly loaded aerospace structures in those days. Fiber-reinforced materials do not pose the restriction of biaxial loading, due to their tailorability and this property led to an increased spatial freedom for pressure vessels that are required to have a high structural efficiency [9–11]. The structural efficiency is defined as the ratio of the mass and the pressurized volume of the pressure vessel. The multicell reservoir was in danger of being overlooked due to the introduction of fiber-reinforced materials, but structural efficient solutions for the applications mentioned in the beginning of the Introduction require articulated pressurized structures. Conformable tanks (multibubble tanks) have been recently manufactured by an Australian company named PPI (Fig. 4) and an American company named ATK (Fig. 5) [12]. The conformable tanks from both companies are optimized with respect to the limitations of their manufacturing processes.[§] These limitations lead to a restricted spatial freedom and the structural efficiency is less than optimal. According to Vasiliev et al. [13], the structural efficiency is optimal when the material from the pressure vessel is in a state of uniform equal biaxial extension, provided that the entire pressure vessel is made from the same material. This means that the principal strains are positive, equal, and uniform over the entire structure. The current conformable tanks from PPI and ATK are not loaded in a state of uniform equal biaxial extension.

No conformable pressure vessels with full spatial freedom, made from high specific strength materials and optimal structural efficiency have yet been realized. The aim of this paper is to investigate the structural concept of a pressure vessel that needs to fit in a dedicated geometrical space; therefore, we outline the concept of the multibubble pressure vessel. in Sec. II, background information is provided that forms a foundation for the chosen shape of the multibubble. The analysis of the multicylinder and the multisphere, which are the membrane elements that form the multibubble in this

Received 1 September 2010; revision received 4 January 2011; accepted for publication 29 January 2011.

*Ph.D. Researcher, Design and Production of Composite Structures, Kluyverweg 1; f.geuskens@tudelft.nl.

†Assistant Professor, Design and Production of Composite Structures, Faculty of Aerospace Engineering, Kluyverweg 1.

‡Professor, Design and Production of Composite Structures, Faculty of Aerospace Engineering, Kluyverweg 1.

§Data available online at http://www.ppidts.com/ [retrieved 5 April 2011].

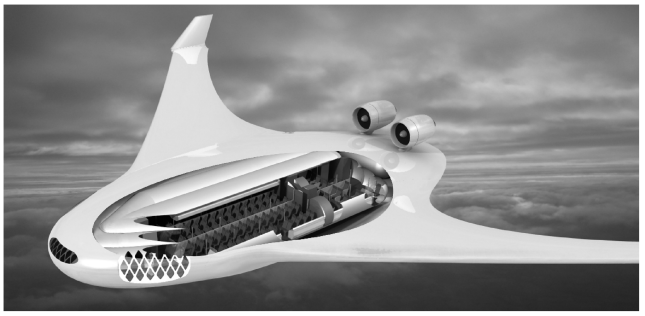

Fig. 1 Pressure-cabin concept for a BWB [18].

paper, are presented in Sec. III. Section IV discusses the applications of the multibubble and outlines future research. Finally, conclusions are given in Sec. V.

II. Background: Stresses in Pressurized Vessels

If the layout of a pressure vessel would be an enclosed space, built up from straight rigid panels, the vessel would be subjected to immense bending stresses when pressurized, thus requiring extra material to lower the stress. A pressure vessel built up from straight panels is therefore a configuration that results in a high weight penalty. To avoid bending stresses, the structure needs to have the ability to carry the pressurization loads by in-plane stresses. Thin-walled shells of revolution have this ability because the cross section in one direction is circular, resulting in in-plane stresses exclusively, as illustrated in Fig. 6. This figure schematically shows the loads acting on pressurized circular and elliptical cylinders.

The loads acting in the wall of the pressure vessel can be visualized by cutting a segment from the cylinder. In Fig. 6, we consider the loads acting on the upper segment. The pressurization load acting on the edge of the segment can be visualized by projecting the pressurization loads on the x and y axes. The projected loads on the x axis (O–A) are counteracted by the vertical membrane force F_Y, and the projected load on the y axis (O–B) is counteracted by the horizontal membrane force F_X. We note that the resultant membrane force F_R always works tangentially in the case of a circular cross section, whereas in the case of a different cross section, such as an elliptic one, part of the resultant force is out of plane. Cylinders that do not have a circular cross section will face bending moments in the skin. The response of pressurized elliptical cylinders is investigated in [14]. The analysis of the bending moment in a pressurized cylinder of an arbitrary (smooth) profile, with two axes of symmetry, has been developed in polar coordinates by Holland [15]. The advantage of structures that carry solely in-plane tension loads is that they show the potential to design the pressure vessel such that the structure is in a uniform equal biaxial extension state, which maximizes the

Fig. 2 Multibubble tank structure tested with cryogenic propellant at NASA Glenn Research Center [4].

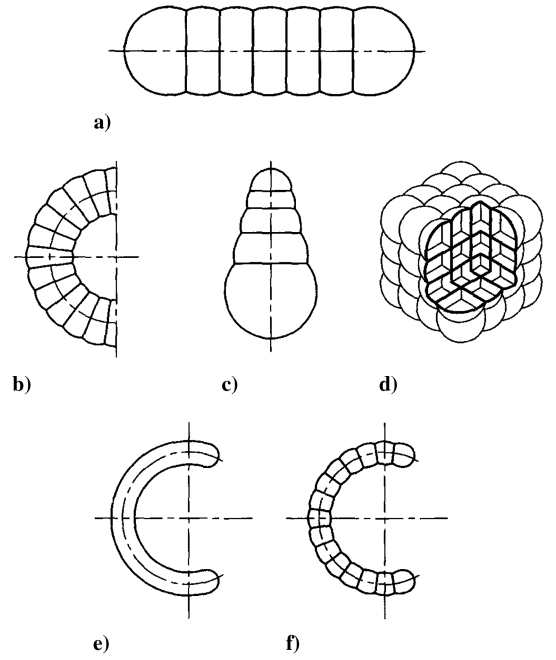

Fig. 3 Illustration of the multispherical structures analyzed by Komarov [8].

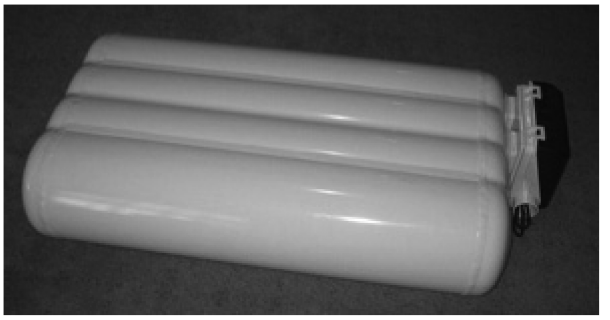

Fig. 4 Conformable tank from PPI (see footnote [§]).

Fig. 5 Prototype two cell conformable tank from Thiokol [12].

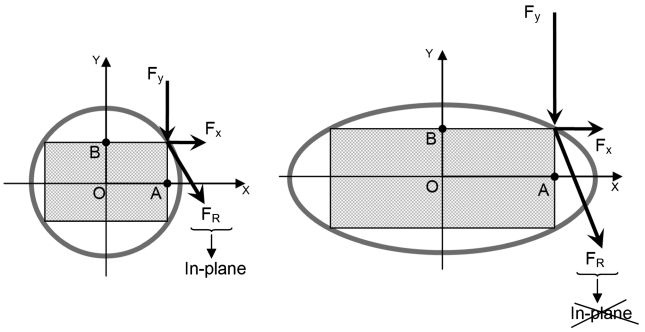

Fig. 6 Load visualization on the edge of the upper segment of a pressurized a) circular cylinder and b) elliptical cylinder.

structural efficiency when the entire vessel is made from the same material [13].

The challenge is to design pressure vessels that can be fit into the space requirements of the system and that can carry pressurization loads solely by in-plane loads.

The multibubble provides the opportunity to meet this challenge [16] and is analyzed in the following sections.

III. Multibubble Concept

The multibubble in this paper is composed of two different membrane elements: 1) the cylinder, which is a constituent of the multicylinder, and 2) the sections that close the multibubble, called the multisphere. The multisphere can be configured in an open-cell or closed-cell configuration. All membrane elements are in this paper assumed to be subjected under uniform internal normal pressure. Multispherical pressure vessels have already been investigated by [5–8], Komarov [7,8] has already investigated multispherical tanks (Fig. 3), but the analysis in this paper is worked out in more detail, and publications of the analysis of multispheres used as bulkheads for multicylinders are unknown until now. Section III explains the analysis of the forces and the loads in the multibubble composed of multicylinders and multispheres as membrane elements. There are multiple arrangements possible, and the most simple arrangement is first analyzed: the single-row multibubble (Fig. 7a). Subsequently, complexity is added by linking single-row multibubbles into a multirow multibubble (Fig. 7b). Finally, the multicell multibubble (Fig. 7c) is analyzed.

A. Single-Row Multibubble

1. Analysis of the Single-Row Multicylinder

The multicylinder design illustrated in Fig. 8 is structurally efficient with respect to balancing the pressurization loads.

The circumferential tension force is given by [17]

$$N_{\phi,c} = pR \tag{1}$$

where p is the internal pressure, R is the radius of the cylinder, and the index c refers to the cylinder. All membrane forces are defined per unit length; multiplying the membrane force with the length gives the total load, and dividing the membrane force with the membrane's thickness gives the average stress in the membrane. The circumferential tension forces where the different radii meet are balanced out by a single wall (Fig. 8).

The membrane force in the wall ($F_{\phi,c}$) at location A is found by considering the equilibrium of forces in the x and y directions:

$$F_{\phi,c} = Y_1 + Y_2 = N_{\phi 1}\cos\phi_1 + N_{\phi 2}\cos\phi_2 \tag{2}$$

where Y_1 and Y_2 are defined as the components in the y direction of the circumferential tension force of the cylinders with R_1 and R_2, respectively. The angle ϕ is defined as the angle between the local x axis and the line that runs from the local origin to the intersection.

The cylinders are dimensioned in such a way that the component in the x direction of the membrane force of one cylinder (X_1) is balanced by the component in the x direction of the membrane force of the neighboring cylinder (X_2).

The membrane forces X_1 and X_2 are defined as

$$X_1 = N_{\phi 1}\sin\phi_1 = pR_1\sin\phi_1 \qquad X_2 = N_{\phi 2}\sin\phi_2 = pR_2\sin\phi_2 \tag{3}$$

To have equilibrium in the x direction at location A, the following condition must be met:

$$R_1\sin\phi_1 = R_2\sin\phi_2 \tag{4}$$

Looking at this equation from a geometrical point of view, it is clear that Eq. (4) is met for every cylinder that is merged on to another cylinder as long as the axes of the cylinders are parallel with respect to each other.

This condition provides considerable flexibility in controlling the geometry of the cross-sectional area. Bubbles with different diameters can be connected and the intersecting walls do not need to

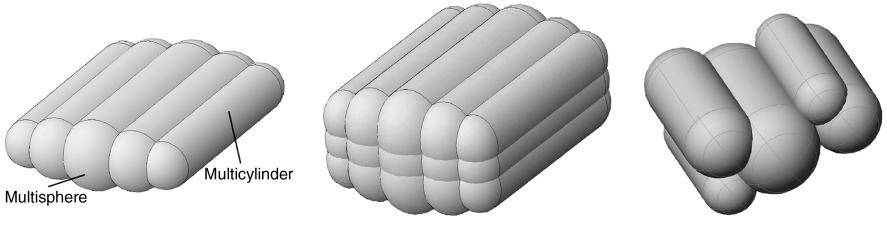

a) Single row **b) Multirow** **c) Multicell**

Fig. 7 Configurations multibubble.

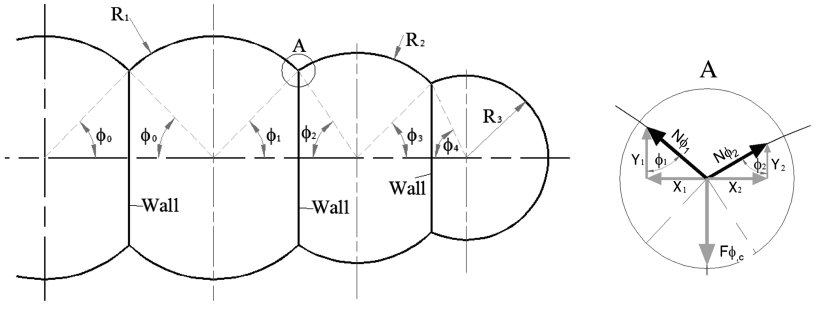

Fig. 8 Layout of a multibubble.

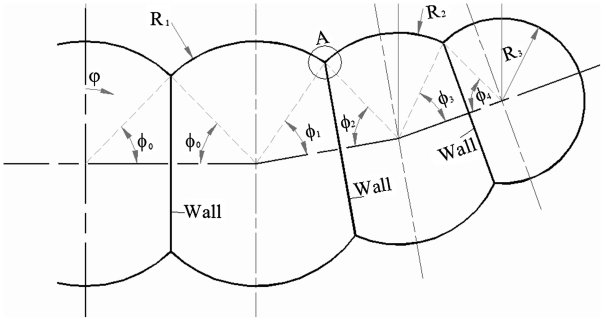

Fig. 9 Variation on the single-row multicylinder.

be vertical. Several bubbles of the multicylinder can be placed higher or lower by rotating these bubbles over the center of the adjacent bubble (Fig. 9). The analysis remains applicable because the local xy coordinate system is also rotated.

The axial force in the multicylinder is induced by the hoop forces of the closing spherical membrane element, defined as [17]

$$N_{\theta,s} = N_{x,c} = \frac{pR}{2} \tag{5}$$

where the index s refers to the sphere. Multiplying this axial force with the arc length s of the membrane and dividing it by the pressure equals an area A^*, which represents the hatched area in Fig. 10:

$$A^* = \frac{N_{x,c} \cdot R(2\pi - 2\phi)}{p} = R^2(\pi - \phi)$$

The axial force in the curved membrane does not resist the full load that is exerted by the pressure on the cross-sectional area. The pressure load exerted on the cross-sectional area is partly carried by the curved membrane and partly by the vertical wall or a separate reinforcement depending on the closed- or open-cell configuration. More clarification on the axial load in the multicylinder is explained in the next section.

2. Analysis of the Single-Row Multisphere

The spheres that close off the multicylinder are also structurally efficient shell-structures with respect to balancing the pressurization loads. Membrane forces for the sphere are given by [17]

$$N_{\phi,s} = N_{\theta,s} = \frac{pR}{2} \tag{6}$$

The condition to obtain equilibrium for the multicylinder [Eq. (4)] also holds for the intersection of the multisphere. The intersection of the multisphere in Figs. 11 and 12 is represented as a semicircle with radius $R \sin \phi$.

The force exerted by the intersecting spherical membranes in radial direction (Figs. 11 and 12) is found in the same way as in Eq. (2):

$$F_{\phi,s} = \frac{pR_1 \cos\phi_1 + pR_2 \cos\phi_2}{2} = \frac{F_{\phi,c}}{2} \tag{7}$$

There are two ways of transferring these forces into the structure: via a reinforcement ring, when the multibubble is an open-cell construction [the reinforcement ring is interpreted as a cable that runs over the intersection on the outside surface of the multibubble (Fig. 11)] and via a semicircular wall (referred to as a *circular wall*), when the multibubble is a closed-cell construction (Fig. 12).

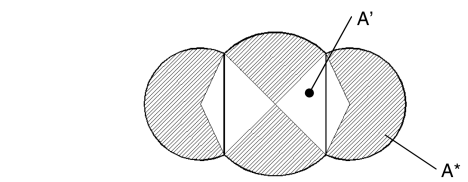

Fig. 10 Equivalent pressure area A^* induced by the axial forces in the multicylinder.

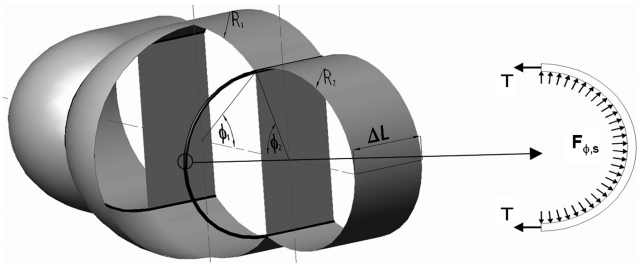

Fig. 11 Open-cell single-row multisphere.

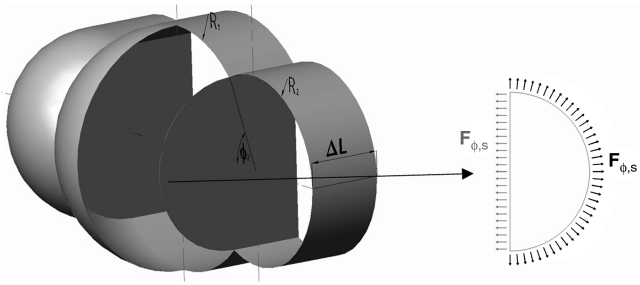

Fig. 12 Closed-cell single-row multisphere.

The choice of the reinforcement depends on the application (open-cell vs closed-cell), the realization of the multibubble, and the material of choice. These choices are further explained in Sec. IV.

For the reinforcement ring, the tensile load in the ring (Fig. 11) is defined as

$$T = R_1 \sin\phi_1 F_{\phi,s} \tag{8}$$

Equilibrium shows that T is equal to the induced load of the remaining pressurized cross-sectional area A' that is illustrated in Fig. 10. The load induced by this area is

$$\text{Load} = p \cdot A' = p \cdot R_1 \sin\phi_1 (R_1 \cos\phi_1 + R_2 \cos\phi_2) = 2T$$

This clarifies the axial load in the multicylinder mentioned in the previous section. The axial load in the multicylinder is carried in the curved membrane and additional reinforcements when the multisphere is configured in an open-cell construction. For this configuration, the vertical wall in the multicylinder and the reinforcement are both uniaxially loaded.

For the closed-cell construction, structural integrity is obtained via a circular wall at the intersection of the spheres. The reactive force is also understood to be $F_{\phi,s}$ and the load induced by this reactive force is derived in the same way as Eq. (8). The difference here is the stress distribution. The circular wall in the multisphere is in an equal biaxial stress state and the stress ratio of the wall in the multicylinder is two [Eq. (7)] for a closed-cell configuration. This means that the stress ratio in the membrane elements of the closed-cell pressurized multicylinder ($N_{\phi,c}$ vs $N_{x,c}$ and $F_{\phi,c}$ vs $F_{\phi,s}$) is exactly the same as the stress ratio for the pressurized cylinder and the same accounts for the closed-cell pressurized multisphere with respect to the sphere.

The practical implications of the closed-cell and the open-cell constructions will be discussed in Sec. IV.

B. Multirow Multibubble

A second configuration of the multibubble is obtained by mirroring (single-row) multibubbles into a multirow multibubble. Application of the multirow multibubble (Fig. 7b) provides the opportunity to maximize the pressurized volume for a pressure vessel that needs to fit within a rectangular cuboidal space.

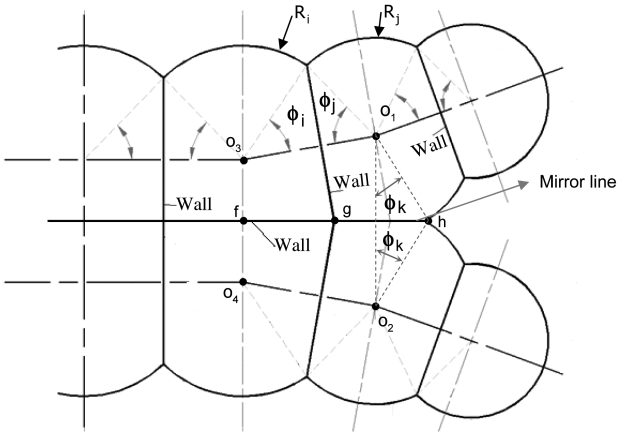

Fig. 13 Double-row multicylinder.

1. Analysis of the Multirow Multicylinder

Similar to the single-row multicylinder, a wall is located at the intersection where the multibubble is mirrored (Fig. 13). The rows or the columns are identical to each other in order to obtain matching intersections at the bulkhead of which the mutual enclosed angle ϕ_k is a result of this constraint (Figs. 13 and 14).

The analysis of the membrane forces in the curved membrane and the wall is identical to the analysis shown in Sec. III.A.1. The analysis of the multicylinder in Fig. 14 is straightforward, but complexity is added for the multicylinder in Fig. 13, because the walls are not all perpendicular with respect to each other.

Looking at the derivations in Sec. III.A from a geometrical point of view, it appears that the membrane forces can be determined as soon as distances (geometry) and pressure are known.

The membrane forces for the multicylinder in Fig. 13 are geometrically derived as

$$N_{\phi,c_i} = p \cdot R_i \tag{9a}$$

$$N_{\phi,c_j} = p \cdot R_j \tag{9b}$$

$$N_{x_i} = \frac{N_{\phi,c_i}}{2} \tag{9c}$$

$$N_{x_j} = \frac{N_{\phi,c_j}}{2} \tag{9d}$$

$$F_{\phi,c_{ij}} = p \cdot |o_1 o_3| \tag{9e}$$

$$F_{\phi,c_{ii}} = p \cdot |o_3 o_4| \rightarrow \text{membrane force in wall } [f,g] \tag{9f}$$

$$F_{\phi,c_{jj}} = p \cdot |o_1 o_2| \rightarrow \text{membrane force in wall } [g,h] \tag{9h}$$

where $|xx|$ denotes the distance between two points. The index ij refers to the intersection between the cylinders with radii R_i and R_j. The axial force in the wall depends on the configuration and is $F_{\phi,s}$ in a closed-cell configuration and zero in an open-cell configuration, due to an additional reinforcement. Explanation is provided in the following section.

2. Analysis of the Multirow Multisphere

For the multirow multisphere, four reinforcement cables merge into one at the intersection of the four spherical membrane elements or four circular walls have one mutual line as the intersection. First, the analysis of the open-cell configuration is shown and the similarities with the closed-cell configuration are explained subsequently. The analysis in this section is first applied to the double-row multibubble displayed in Fig. 14. The more complex multirow multibubble in Fig. 13 is treated subsequently.

The loads in the reinforcement cables and circular walls are derived in the same way as in Sec. III.A.2.

The forces in the radial direction ($F_{\phi,s_{ij}}$, F_{ϕ,s_k}, and F_{ϕ,s_q}) are defined as

$$F_{\phi,s_{ij}} = \frac{pR_i \cos\phi_i + pR_j \cos\phi_j}{2} \tag{10a}$$

$$F_{\phi,s_k} = \frac{pR_j \cos\phi_k + pR_j \cos\phi_k}{2} = pR_j \cos\phi_k \tag{10b}$$

$$F_{\phi,s_q} = pR_i \cos\phi_q \tag{10c}$$

Again, the index ij refers to the intersection enclosed by the angles ϕ_i and ϕ_j, and the index k refers to the intersection in between the mutual enclosed angle ϕ_k. The index q refers to the intersection in between the cylinders with radius R_i, of which the parameter of interest is the mutual enclosed angle ϕ_q (Figs. 14 and 15).

These forces result in tensile loads in their corresponding reinforcement rings, as we have shown in Eq. (8):

$$T_{ij} = F_{\phi,s_{ij}} \cdot R_j \sin\phi_j \tag{11a}$$

$$T_k = F_{\phi,s_k} \cdot R_j \sin\phi_k \tag{11b}$$

$$T_q = F_{\phi,s_q} \cdot R_i \sin\phi_q \tag{11c}$$

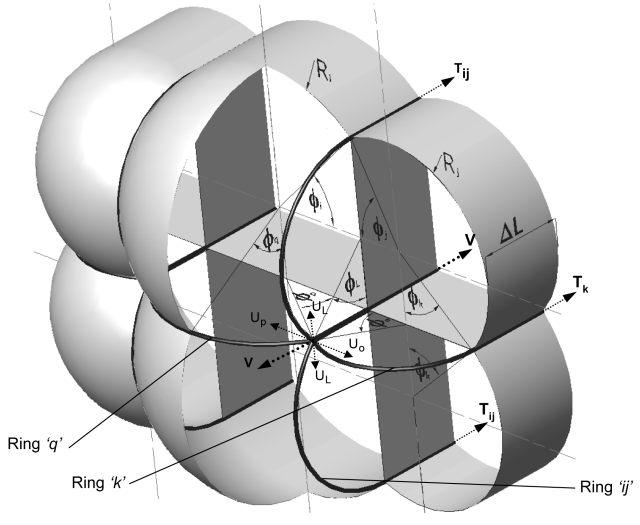

Fig. 14 Open-cell double-row multibubble.

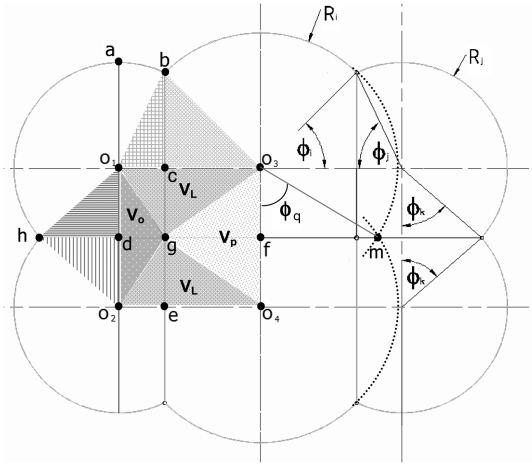

Fig. 15 Geometrical representation of the loads and forces of the multibubble in Fig. 10.

The transversal components (U_L, U_o, and U_p) of these tensile loads need to be in equilibrium, in order to ensure that this multisphere configuration works. The transversal components are defined as

$$U_L = T_{ij} \sin \phi_L \qquad U_o = T_k \sin \phi_o \qquad U_p = T_q \sin \phi_p$$

The equilibrium condition of the transversal components is similar with the equilibrium condition of the multicylinder [Eq. (4)]. This means that the following condition should be met:

$$U_L = U_L \quad \text{(trivial)} \qquad U_o = U_p$$

A closer look at the geometry in Fig. 14 proves that this condition is met. From the geometry, we note that $R_j \cos \phi_k = R_i \cos \phi_q$, meaning $F_{\phi,s_k} = F_{\phi,s_q}$ and $R_j \sin \phi_k \sin \phi_o = R_i \sin \phi_q \sin \phi_p$; hence, $U_o = U_p$.

The axial components of the tensile loads at the intersection of the four rings are defined as

$$V_L = T_{ij} \cos \phi_L \tag{12a}$$

$$V_o = T_k \cos \phi_o \tag{12b}$$

$$V_p = T_q \cos \phi_p \tag{12c}$$

The total axial load induced at the intersection by the four reinforcement rings are

$$V = 2V_L + V_o + V_p \tag{13}$$

It is obvious that these axial loads also represent loads induced by pressurized areas. Deriving the geometrical relations for ϕ_L, ϕ_O, and ϕ_q, we get

$$R_j \sin \phi_j \cos \phi_L = R_j \cos \phi_k$$
$$R_j \sin \phi_k \cos \phi_o = R_j \cos \phi_j$$
$$R_i \sin \phi_q \cos \phi_p = R_i \cos \phi_i$$

Simplifying this yields

$$\cos \phi_L = \frac{\cos \phi_k}{\sin \phi_j} \qquad \cos \phi_o = \frac{\cos \phi_j}{\sin \phi_k} \qquad \sin \phi_q \cos \phi_p = \cos \phi_i$$

By substitution of Eq. (10) in Eq. (11), subsequent substitution in Eq. (12), and by making use of the geometrical relations, we can clearly observe (in Fig. 15) the pressurized areas that the loads V_L, V_o, and V_p represent.

It was already discussed in the previous section that the membrane forces and the loads in the reinforcements can be determined once the geometry (distances and areas) and the pressure are known.

Summarizing this for the multibubble shown in Figs. 14 and 15 (which is symmetrical for convenience), the membrane forces are geometrically derived as

$$N_{\phi,c_i} = p \cdot |o_3 b| \tag{14a}$$

$$N_{\phi,c_j} = p \cdot |o_1 b| \tag{14b}$$

$$N_{\phi,x_i} = \frac{p \cdot |o_3 b|}{2} \tag{14c}$$

$$N_{\phi,x_j} = \frac{p \cdot |o_1 b|}{2} \tag{14d}$$

$$N_{\phi,s_i} = N_{\theta,s_i} = N_{x_i} \tag{14e}$$

$$N_{\phi,s_j} = N_{\theta,s_j} = N_{x_j} \tag{14f}$$

$$F_{\phi,c_{ij}} = 2F_{\phi,s_{ij}} = p \cdot (|o_1 c| + |c o_3|) = p \cdot |o_1 o_3| \tag{14g}$$

$$F_{\phi,c_{kk}} = 2F_{\phi,s_k} = p \cdot (|o_1 d| + |d o_2|) = p \cdot |o_1 o_2| \tag{14h}$$

$$F_{\phi,c_{qq}} = 2F_{\phi,s_q} = p \cdot |o_3 o_4| \tag{14i}$$

where $F_{\phi,s_{ij}}$, F_{ϕ,s_k}, and F_{ϕ,s_q} are the forces experienced by circular wall ij, circular wall k, and circular wall q, respectively, in the case of a closed-cell configuration. In the case of a closed-cell construction, circular walls ij, k, and q are the replacements of ring ij, ring k, and ring q, respectively (Fig. 14). For the closed-cell configuration, the forces $F_{\phi,s_{ij}}$, F_{ϕ,s_k}, and F_{ϕ,s_q} are also the axial forces working on the wall of the multicylinder.

Doing a similar analysis for the closed-cell multirow multisphere, it is shown that the reactive loads induced by the distributed forces on the edges of the circular walls are exactly the same as the loads T_{ij}, T_q, T_k, U_L, U_O, U_P, V_L, V_O, and V_P. The loads are explained by zooming in on circular wall ij (Fig. 16), which replaces reinforcement ring ij in Fig. 14 when the multibubble is a closed-cell multibubble.

The loads induced by the distributed forces on this circular wall are derived as

$$F_{\phi,s_{ij}} \cdot |bc| = F_{\phi,s_{ij}} \cdot R_j \sin \phi_j = T_{ij}$$

$$F_{\phi,s_{ij}} \cdot |cg| = F_{\phi,s_{ij}} \cdot R_j \sin \phi_j \cos \phi_j = V_L$$

$$F_{\phi,s_{ij}} \cdot R_j \sin \phi_j \sin \phi_L = U_L$$

The similarity between the rings and the circular walls is obvious, because the loads induced by the distributed forces in the circular walls equal the loads in the rings. The equilibrium condition also therefore holds at the mutual intersection of the circular walls.

In the case of an open-cell configuration, the loads in the reinforcements are geometrically derived as

$$T_{ij} = p \cdot ([o_1 bc] + [cbo_3]) = p \cdot [o_1 bo_3] \tag{15a}$$

$$T_k = p \cdot [o_1 hd] + [dho_2] = p \cdot [o_1 ho_2] \tag{15b}$$

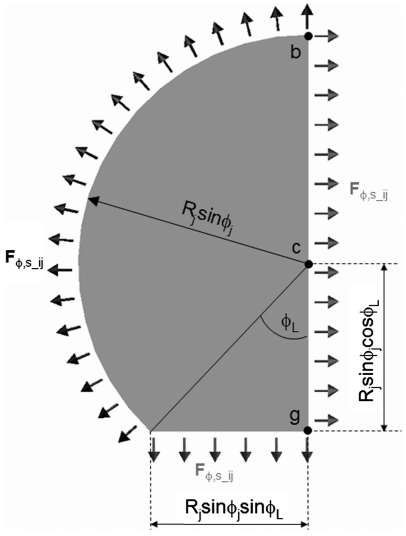

Fig. 16 Visualization of the forces acting on circular wall *ij*.

$$T_q = p \cdot [o_3 m o_4] = \frac{p \cdot (|o_3 f| + |f o_4|) \cdot \sqrt{R_i^2 - |o_3 f|^2}}{2} = \frac{p \cdot |o_3 o_4| \cdot \sqrt{|o_3 b|^2 - |o_3 f|^2}}{2} \tag{15c}$$

$$V = p \cdot ([o_1 o_2 g] + [o_1 o_3 g] + [o_3 o_4 g] + [o_2 o_4 g]) = p \cdot [o_1 o_3 o_4 o_2] \tag{15d}$$

where $|xx|$ denotes de distance between two points, $[xxx]$ denotes the area of the triangle governed by three points, $[xxxx]$ denotes the area of the rectangle governed by four points. The membrane forces are defined as force per unit length, and the loads in the reinforcements are pure forces.

The plane to determine the area that corresponds with T_q is not visible in Fig. 15. This area can be visualized by the area of the triangle created by the points o_3 and o_4 and the apparent intersection m (Fig. 15). The area of the triangle can also be calculated by making use of the Pythagorean theorem.

Equations (14) and (15) provide all the necessary relations to quantify the forces and the loads in, respectively, the membranes and the reinforcements of the multirow multibubble.

It was already discussed in the previous section that the multibubble in Fig. 13 has an additional complexity, because the walls are not perpendicular with respect to each other. For the same analysis, the forces and loads working on the pressurized multibubble of Fig. 13 can easily be represented in a geometric way, as shown in Fig. 17. Equations (14) and (15) also apply for the multibubble in Fig. 17. The only difference for this multibubble is that the rectangle $[o_1 o_3 o_4 o_2]$ is now a trapezium.

C. Multicell Multibubble

The multibubble in Figs. 18 and 19 is a configuration in which the cells are randomly connected with each other. For this configuration, there are three walls and three reinforcement rings that intersect each other. This configuration provides the opportunity to pressurize a volume with substantial spatial freedom (Fig. 7c).

1. Multicell Multicylinder

The walls in the multicylinder in Fig. 19 are formed by the apparent intersections of the cells (dotted lines) and run until the intersecting wall is intersecting another wall (solid lines).

The derivations of the membrane forces in the curved sections and the intersecting walls of the multicell multicylinders remain identical with the derivations presented in the previous sections.

The geometrical complexity of the multicell multibubble is higher, and it is therefore more convenient to define the loads and the membrane forces according to the geometry, depicted in Eq. (14).

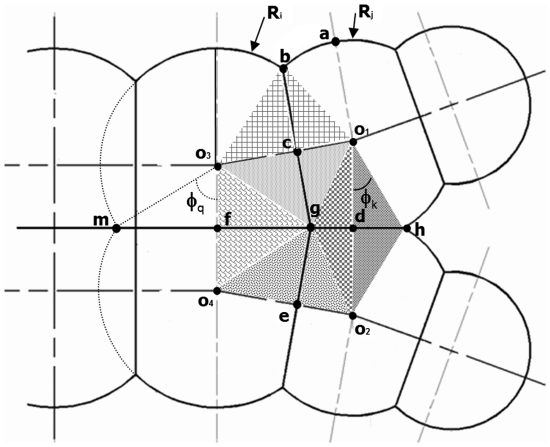

Fig. 17 Geometrical representation of the loads of the multirow multibubble of Fig. 9.

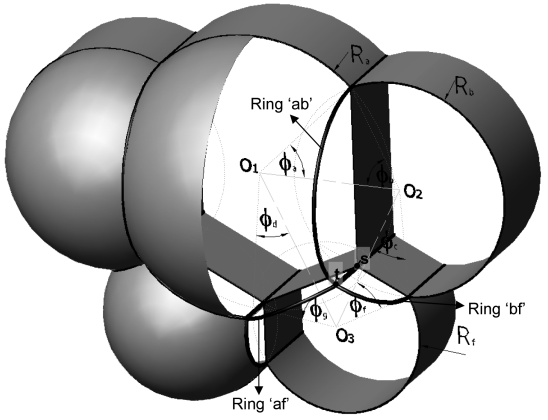

Fig. 18 Example of a open-cell multicell multibubble.

Taking three interconnected cells into consideration, the membrane forces for these cells (Fig. 19) are defined as

$$N_{\phi,c_a} = pR_a \tag{16a}$$

$$N_{\phi,c_b} = pR_b \tag{16b}$$

$$N_{\phi,c_f} = pR_f \tag{16c}$$

$$N_{\phi,x_a} = \frac{pR_a}{2} \tag{16d}$$

$$N_{\phi,x_b} = \frac{pR_b}{2} \tag{16e}$$

$$N_{\phi,x_f} = \frac{pR_f}{2} \tag{16f}$$

$$N_{\phi,s_a} = N_{\theta,s_a} = N_{x_a} \tag{16g}$$

$$N_{\phi,s_b} = N_{\theta,s_b} = N_{x_b} \tag{16h}$$

$$N_{\phi,s_f} = N_{\theta,s_f} = N_{x_f} \tag{16i}$$

$$F_{\phi,c_{ab}} = 2F_{\phi,s_{ab}} = p \cdot |o_1 o_2| \tag{16j}$$

$$F_{\phi,c_{bf}} = 2F_{\phi,s_{bf}} = p \cdot |o_2 o_3| \tag{16k}$$

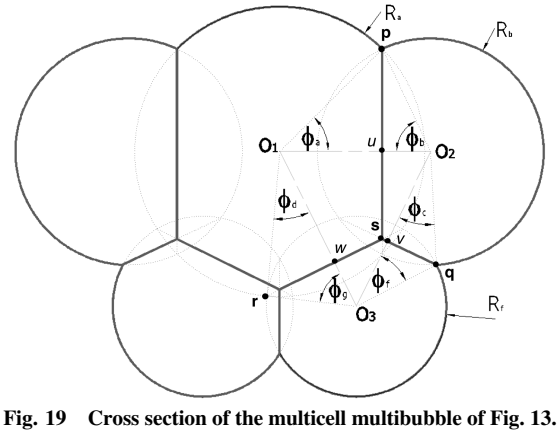

Fig. 19 Cross section of the multicell multibubble of Fig. 13.

Fig. 20 Soap bubbles: an example of the spatial freedom of a closed-cell multisphere.

$$F_{\phi,c_{fa}} = 2F_{\phi,s_{fa}} = p \cdot |o_3 o_1| \tag{16l}$$

The membrane forces $F_{\phi,c_{ab}}$, $F_{\phi,c_{bf}}$, and $F_{\phi,c_{fa}}$ are in equilibrium, since the triangle $[o_1 o_2 o_3]$ is a closed triangle.

2. Analysis of the Multicell Multisphere

The methodology to derive the loads in the reinforcements of the multisphere relies on the derivations in the previous sections. Because of the complexity of the geometry, it is also more convenient to express the loads in terms of areas, as with Eq. (15). The loads in the reinforcements for the multisphere in Fig. 18 are

$$T_{ab} = p \cdot [o_1 p o_2] \tag{17a}$$

$$T_{bf} = p \cdot [o_2 q o_3] \tag{17b}$$

$$T_{af} = p \cdot [o_1 r o_3] \tag{17c}$$

$$V = p \cdot ([o_1 s o_2] + [o_2 s o_3] + [o_3 s o_1]) = p \cdot [o_1 o_2 o_3] \tag{17d}$$

It seems that the reinforcements of the multisphere are in equilibrium when the corresponding walls of the multicylinder are in equilibrium. To prove this, we consider the transversal components of the reinforcement cables, defined as

$$U_h = \frac{F_{\phi,c_{ab}}}{2} \cdot R_a \sin\phi_a \sin\phi_h$$

$$U_i = \frac{F_{\phi,c_{bf}}}{2} \cdot R_b \sin\phi_c \sin\phi_i$$

$$U_j = \frac{F_{\phi,c_{af}}}{2} \cdot R_f \sin\phi_g \sin\phi_j$$

Taking a closer look at the geometry, we observe that (Fig. 18)

$$R_a \sin\phi_a \sin\phi_h = R_b \sin\phi_c \sin\phi_i = R_f \sin\phi_g \sin\phi_j = |ts|$$

This means that the multisphere is in equilibrium when the membrane forces in the walls are in equilibrium, which was already proven in Sec. III.C.1.

When the open-cell multisphere is replaced by a closed-cell multisphere, the rings are replaced by circular walls of which the circular walls are passing through the intersections of the spheres. The methodology to derive the forces in the circular walls was already explained in Sec. III.C.2. The forces in the circular walls are defined in Eq. (16).

A cluster of soap bubbles (Fig. 20) is the perfect example of the tremendous amount of spatial freedom that the multisphere offers. The multisphere can be analyzed step by step by taking three interconnected spheres into consideration, in which the reference plane is the plane that goes through the centers of the three spheres.

IV. Discussion

In Sec. III, it was mentioned that the configuration of the multisphere determines if the multibubble is in a closed-cell or open-cell configuration. The configuration depends primarily on the application.

The open-cell is interesting when the multibubble has to offer usable space (Figs. 1 and 21). For the blended-wing–body pressure cabin, the open-cell configuration is chosen for passenger acceptance and orientation and evacuation issues [18]. The functionality of the wall in the multicylinder in Fig. 21 is replaced by pillars and beams that run over the intersection outside the cabin. The beams are detrimental for the structural efficiency [19], however, and a way to avoid this is by making a pressure cabin that is built up from open-cell multispheres. There are advantages and disadvantages in the tradeoff between the open-cell multisphere and the multicylinder with beams and pillars. The multicylinder with pillars provides more usable space, the single curved membrane is easier to manufacture and the open-cell multisphere offers better structural efficiency.

The closed-cell configuration is interesting when the multibubble is used as a pressure vessel (Figs. 4 and 5). The closed-cell configuration minimizes the impact on local leaks and simplifies the manufacturing process if liners or gas-impermeable bags are used in the multibubble. The conformable tank in Fig. 4 is intended to be used as a tank for liquefied petroleum gas for the automotive industry. The conformable tank from PPI is a very clever design for the application for which it is intended. The end domes have torispherical heads, because spherical heads require excessive forming during fabrication, there are no liners needed and the tank is made from aluminum, which makes the design cost-effective. Because of the limitations of the manufacturing process, the structural efficiency of the tank in Fig. 4 is less than optimal, however, and the diameters of all the cylinders have to be the same, because torispherical end domes are chosen to close the conformable tank.

Vasiliev et al. [13] showed that the structural efficiency of a pressure vessel is optimal when the structure is in a state of uniform equal biaxial extension, provided that the vessel is made out of the same material. The structural efficiency is in that case derived to be

$$\frac{PV}{m} = \frac{\sqrt{\sigma_1^2 + \sigma_2^2}}{3\rho} \tag{18}$$

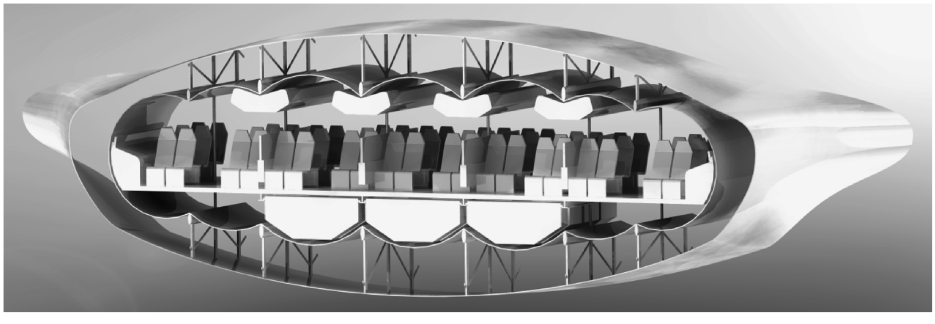

Fig. 21 Layout of the multicylinder in the pressure cabin of the blended wing–body.

The structural efficiency is defined as the ratio of the pressurized volume $P \cdot V$ and the mass m of the pressure vessel. The structural efficiency depends on the density ρ of the material of the pressure vessel and on the allowable tensile stresses in the principal stress directions. These are the circumferential and axial stresses for the multicylinder and the circumferential/meridional and hoop stresses for the multisphere. Note that in this derivation [13], it is assumed that the allowable stresses σ_1 and σ_2 correspond with equal strain. This is valid for isotropic materials, but it is not necessarily true for anisotropic materials. Equation (18) is always valid when the maximum strain criterion is used as the failure criterion for anisotropic materials. Equation (18) does not show geometrical parameters. This means that the structural efficiency is the same for any pressurized shape when the material is in a state of uniform equal biaxial extension. Equation (18) shows that pressurized gas tanks can be made smaller by increasing the pressure, whereas the weight remains the same. Manufacturing multiple individual bottles is less complicated than manufacturing a multibubble. This is why the application of the multibubble is mainly restricted to cryogenic and liquid gas tanks (because the compressibility is not proportional with the volume reduction) and to pressure cabins.

The optimal pressure vessel with substantial spatial freedom made of isotropic materials is a closed-cell multisphere. Welding all the membrane elements together makes the structure prone to flaws, however, and it is an expensive process. The multibubble in Fig. 4 is easier to manufacture (see footnote [§]), but there is less structural efficiency, because the material of the multicylinder and the torus in the torispherical end dome are not in a state of equal biaxial strain.

A better strain distribution can be achieved by making the multibubble from fiber-reinforced materials (Fig. 5), because the tailorability of the composites allows the fibers to be to directed and sized according to the orientation and the magnitude of the principal stresses (assuming that the fibers are the only load-carrying elements). Another advantage of uniform equal biaxial strain is the fact that there is strain compatibility at the intersections of the different membrane elements, which avoids bending and stability issues. Although strain compatibility does not necessarily mean that the structural efficiency is optimal, it is a very important aspect with respect to ensuring structural integrity.

Composite multibubbles require solutions for several manufacturing challenges. It is difficult to manufacture quasi-isotropic spherical membranes, and fibers are generally oriented in a plane that makes it difficult to manufacture the intersections of the multibubbles shown in Sec. III. ATK [20] (Figs. 5 and 22) bypassed this difficulty by altering the design such that the membrane forces X_1 and X_2 [Eq. (3)] are zero at the intersections. This can be achieved by making the radius of curvature at the intersection (r) of the individual bubbles smaller than the large radius of the two outer bubbles (R) (Fig. 22). In this way, the conformable tank can be a composition of individual filament wound cells. The individual cells comprising the tank are wound with a combination of hoop and helical composite layers. The individual cells are then joined together to form a complete tank using winding tooling that allows a final hoop overwrap to be wound over the cylindrical part of all the cells. The membrane force in the hoop overwrap for this tank is derived as

$$N_{\text{hoop}} = p \cdot d$$

where d is the distance defined in Fig. 22.

The end domes of the conformable tank combine different curvatures for the same layup, which implies that all elements of the material of the conformable cannot be in an equal biaxial strain state. Although the penalty is relatively small, this means that the structural efficiency is less than optimal. The limitation that both conformable tanks from PPI and ATK (Figs. 4 and 5) have is that, due to the limitations of the manufacturing processes, the design does not allow the spatial freedom as is displayed in Figs. 9 and 18.

The aspects that have to be investigated in future research are the realization of multibubbles with full spatial freedom, strain compatibility, and the effect on the structural efficiency of different structural configurations, as well as expanding the multibubble with different membrane elements such as the multicone, the multitorus, and other multismooth shells of curvature.

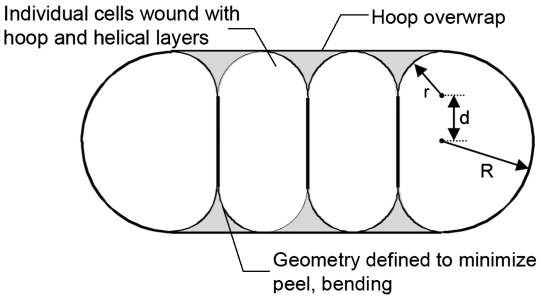

Fig. 22 Composite conformable tank configuration from ATK [12].

V. Conclusions

This paper introduces the multibubble concept and presents the structural analysis methodology. The multibubble is an articulated pressurizable structure that enables pressurization of a volume with substantial spatial freedom. It has been shown that a multibubble membrane element requires circular cross sections in order to counteract pressurization loads solely by in-plane stresses, thereby providing the ability to design a structurally efficient pressure vessel. To demonstrate this principle, a multibubble composed of cylindrical and spherical membrane elements is analyzed here. The multibubble in this paper can be configured in an open- or closed-cell configuration. It is also demonstrated that the structural integrity of the closed-cell multibubble is maintained by walls. A conclusion from the analysis of the closed-cell multibubble is that the stress ratio in the membrane elements of the closed-cell pressurized multicylinder is exactly the same as the stress ratio for the pressurized cylinder, and the same accounts for the closed-cell pressurized multisphere with respect to the pressurized sphere. The structural integrity of the open-cell multibubble is maintained by a uniaxial loaded wall for the multicylinder and uniaxial loaded reinforcements at the intersections of the cylindrical and spherical elements. Finally, it is demonstrated that the forces and loads in the multisphere and multicylinder can easily be defined once the pressure, dimensions, and areas in the corresponding cross section are known.

References

[1] Mukhopadhyay, V., "Structural Concepts Study of Non-Circular Fuselage Configurations," SAE International, Paper SAE WAC-67, Oct. 1996.

[2] Potsdam, M. A., Page, M. A., and Liebeck, R. H., "Blended Wing Body Analysis and Design," AIAA 15th Applied Aerodynamics Conf., Atlanta, AIAA Paper 1997-2317, 1997.

[3] Mukhopadhyay, V., Sobieszczanski-Sobieski, J., Kosaka, I., Quinn, G., and Vanderplaats, G., "Analysis, Design, and Optimization of Non-Cylindrical Fuselage for Blended-Wing-Body Vehicle," *Journal of Aircraft*, Vol. 41, No. 4, July–Aug. 2004, pp. 925–930. doi:10.2514/1.417

[4] "Final Report of the X-33 Liquid Hydrogen Tank Test Investigation," NASA Marshall Space Flight Center, Huntsville, AL, May 2000.

[5] Jackson, J. O., and Stone, C. L., "Intersecting Spherical Pressure Tank," U.S. Patent 2341044, issued 8 Feb. 1944.

[6] Bert, W. C., "Large Weight Reductions Possible in Pressure Vessels," *Space/Aeronautics*, Vol. 38, No. 5, 1962, pp. 77–83.

[7] Komarov, V. A., "Multicell Reservoir," *Mechanics of Solids*, Vol. 5, 1970, pp. 181–183.

[8] Komarov, V. A., "Multispherical Structures—Properties and Application," *Polyot*, No. 10, 2007, pp. 41–43 (in Russian).

[9] Vasiliev, V. V., *Composite Pressure Vessels—Analysis, Design, and Manufacturing*, Bull Ridge, Blacksburg, VA, 2009.

[10] Gerard, G., "Comparative Efficiencies of Aerospace Pressure Vessel Design Concepts," *AIAA Journal*, Vol. 4, No. 12, 1966, pp. 2081–2089. doi:10.2514/3.3859

[11] Love, G. G., "Structural Analysis of Orthotropic Shells," *AIAA Journal*, Vol. 1, No. 8 1963, pp. 1843–1847. doi:10.2514/3.1933

[12] Haaland, A., "High-Pressure Conformable Hydrogen Storage for Fuel

Cell Vehicles," *Proceedings of the 2000 Hydrogen Program Review*, NREL CP-570-28890.

[13] Vasiliev, V. V., Krikanov, A. A., and Razin, A. F., "New Generation of Filament-Wound Composite Pressure Vessels for Commercial Applications," *Composite Structures*, Vol. 62, Nos. 3–4, 2003, pp. 449–459. doi:10.1016/j.compstruct.2003.09.019

[14] McMurray, J. M., and Hyer, M. W., "Response and Failure Characteristics of Internally Pressurized Elliptical Composite Cylinders," *AIAA Journal*, Vol. 40, No. 1, 2002, pp. 117–125. doi:10.2514/2.1620

[15] Holland, M., "Pressurized Non-Circular Member—Effect of Mean-Line Form," *Journal of Strain Analysis for Engineering Design*, Vol. 17, No. 4, 1982, pp. 237–241. doi:10.1243/03093247V174237

[16] Beukers, A., and van Hinte, E., *Flying Lightness, Promises for Structural Elegance*, 010 Publishers, Rotterdam, 2005.

[17] Flűgge, W., *Stresses in Shells*, 3rd ed., Springer–Verlag, Berlin, 1960, Chap. 2.

[18] Van der Voet, Z., "Conceptualisation of a Future Passenger Aircraft Interior Using a Non-Cylindrical Pressure Fuselage," M.S. Thesis, Delft Univ. of Technology, Delft, The Netherlands, 2009.

[19] Geuskens, F. J. J. M. M., Koussios, S., and Bergsma, O. K., "Composite Pressure Fuselages for Blended Wing Bodies," *ICCM Conference 2009*, Edinburgh, Scotland, U.K., 2009.

[20] Gold, R. P., Kunz, R. K., and Warner, M. J., "The Shape of Things to Come," *SAMPE Journal*, Vol. 35, No. 2, March–April 1999, pp. 10–18.

S. Pellegrino
Associate Editor